PCCP

Accepted Manuscript

ROYAL SOCIETY OF CHEMISTRY

www.rsc.org/pccp

Journal Name

ARTICLE

Assembly of Ag_3PO_4 Nanoparticles on Two-dimensional Ag_2S Sheets as Visible-Light-Driven Photocatalysts

Received 00th January 20xx,
Accepted 00th January 20xx

DOI: 10.1039/x0xx00000x

www.rsc.org/

Peiyan Ma[a], Hongjian Yu[b], Yong Yu[a], Weimin Wang[b], Hao Wang[b], Jinyong Zhang[b] and Zhengyi Fu [b,†]

Ag_3PO_4 has been proven to be a promising catalyst with superior activity compared to other existing visible-light-driven photocatalysts. In this work, Ag_3PO_4 nanoparticles were deposited on the surface of two-dimensional Ag_2S sheets by in-situ synthesis strategy. The microstructure, composition, and performance of the resulting Ag_3PO_4/Ag_2S composites could be tailored by surface-functioned Ag_2S sheets. The composite reached optimum performance when the molar ratio of Ag_2S to Ag_3PO_4 was 0.31, showing a 2-fold enhancement in the degradation rate in comparison to pure Ag_3PO_4. Efficient separation of photogenerated electron-hole pairs was achieved through a Z-scheme system in which Ag particles served as the center for the combination of electrons at the conduction band of Ag_3PO_4 and holes at the valence band of Ag_2S. In addition to the matched band structure of Ag_2S and Ag_3PO_4, the monodisperse Ag_3PO_4 nanoparticles were efficient in light harvesting due to the presence of Ag_2S. The advantageous interface effect produced by Ag_2S sheets and nano-sized Ag_3PO_4 nanoparticles also contributed to the improvement in photocatalytic activity.

1. Introduction

Recently, the urgent desire for the high-performance photocatalysts to handle organic pollutes in waters has triggered the research upsurge in Ag_3PO_4, which has high quantum efficiency and excellent activity in the decomposition of organic dyes under visible light illumination.[1, 2] More efforts have been concentrated on the regulation of its microstructure, the synthesis of Ag_3PO_4-based composite materials,[3-5] as well as the exploration of the catalytic mechanism. Different measures have been taken to improve the catalytic efficiency of Ag_3PO_4, such as the synthesis of organic-inorganic hybrid nanocomposites, [6] the development of Z-Scheme photocatalysis systems [7], and the application of heterogeneous photocatalysis systems.[8-10]Although the catalytic activity of Ag_3PO_4 has been enhanced to a certain degree, vital problems regarding the stability and electron-hole recombination of silver compounds remain the technical barriers for its practical application.

Despite the abundantly active centres, the significant enhancement of catalytic activity, and the proven synthesis methods, nano-sized photocatalysts have always been excluded for the unfavourable factors, such as agglomeration, inactivity, and recycling difficulty. Moreover, it is a tough task to remove the crystal growth inhibitors due to the high cost and technical deficiencies. Previous research suggests that surface-functionalized two-dimensional materials can not only induce the growth of nano photocatalysts but also stabilize them in the complicated reaction processes. Typically, graphene oxide with abundantly oxygen-containing groups makes it feasible. AgCl, AgBr, CdS, Hematite, Ag, and Au nanomaterials have been combined with graphene oxide or graphene in this way.[11-16] Due to the synergistic effect of two-dimensional carriers and nanoparticles generated at the interface, the obtained composites showed enhanced properties compared to the single sample. Another π-conjugated semiconductor material, g-C_3N_4, can also induce the in- situ deposition of nanoparticles and participate in the photoelectric reactions.[6, 17-20] Inspired by these exploratory researches, surface-functionalized two-dimensional materials with matched band structure should be applied as the carriers for nano Ag_3PO_4 materials. These two-dimensional materials could exert positive effect on the photocatalytic efficiency.

Monoclinic α-Ag_2S, a direct semiconductor with a band gap of ~1.0 eV, possesses a high absorption coefficient and excellent conductivity properties. Consequently, the Ag_2S quantum dots covering the absorption range from visible to infrared area are favourable sensitizers for ZnO and TiO_2 photoelectric materials.[21, 22] Notably, the morphology, structure, and properties of Ag_2S can be adjusted by solution-related methods. For instance, Ag_2S-based composites and heteronanostructures were fabricated by sulfuration of silver and AgCl particles.[23]Ag_2S nanofibers applied on an electrical transfer and switching device were synthesized with sacrificial $Ag_2C_2O_4$ as the template.[24] Ag_2S superlattices were successfully

[a] School of Chemistry, Chemical engineering and Life science, Wuhan University of Technology, Wuhan, Hubei 430070, PR China.
[b] State Key Lab of Advanced Technology for Materials Synthesis and Processing, Wuhan University of Technology, Wuhan, Hubei 430070, PR China.
† E-mail: fuzhengyi@whut.edu.cn.
Electronic Supplementary Information (ESI) available: See DOI: 10.1039/x0xx00000x

assembled with nanoscale hollow spheres via microemulsion-based synthesis and phase-separation reactions.[25] Additionally, α-Ag_2S has a feature of stability because it can maintain structural integrity in water for a long time with a barely perceptible dissolution of Ag^+(K_{sp}^{Θ}= 6.3×10^{-50}, 25°C). Furthermore, it can be hybridized with organic functional materials.[26,27] In consideration of the above discussion, we choose Ag_2S as a potential carrier for targeted nanomaterial.

In this paper, we present a novel method to fabricate Ag_3PO_4/ Ag_2S composite using porous Ag_2S sheets as the support at room temperature. Ag_2S sheets were transformed from ZnS-ethanediamine (ZnS-en) hybrid by cation-exchange technology. The illustration of preparation process is shown in Fig.1. We focused on the structural characteristics of the composites formed with nano-size Ag_3PO_4 particles on the surface of two-dimensional Ag_2S sheets, the structure-properties relation, and the corresponding catalysis mechanism. The research will provide solutions to the limiting factors of Ag_3PO_4 and improve its photocatalytic performance. The related results mean that our strategies are feasible and offer a reference for the development of Ag_3PO_4-based composites.

2. Experimental

2.1. Materials

All the chemicals were obtained from Sinopharm Chemical Reagent Co., Ltd. (Shanghai, China). The materials were used as received without further treatment.

2.2 Preparation of photocatalysts

2.2.1 Preparation of two-dimensional ZnS-ethanediamine (ZnS-en) hybrid

ZnS-en hybrid was synthesized according to the method released by L. Nasi et al.[28] In a typical synthesis, 1 mmol zinc nitrate and 2 mmol thiourea were dissolved in a mixed solvent (30 mL of ethanediamine and 2 mL of deionized water). The mixed solution was magnetically stirred for 15 min, then sealed in a hydrothermal reactor (50 mL capacity) and heated at 140°C for 12 h. Thereafter, the solid product was collected by centrifugation, and then washed with deionized water and absolute ethanol for several times. Finally, the sample was dispersed in 50 mL of deionized water.

2.2.2 Preparation of two-dimensional Ag_2S-en hybrid

80mL of $AgNO_3$ solution (0.05mol/L) was added to the above solution, and then the mixture was heated in a water bath at 90°C for 2 h. In this process, the precipitate turned from white to black, indicating the successful transformation from ZnS to Ag_2S. The black sample was washed with 0.1 M HCl solution to dissolve unreacted ZnS, then washed with deionized water, and finally dried in vacuum at 30°C for a whole night.

2.2.3 Preparation of Ag_3PO_4/Ag_2S composites

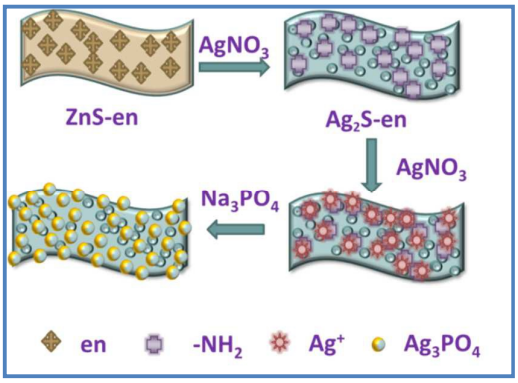

Fig.1 Illustration of in- situ deposition of Ag_3PO_4 nanoparticles on the surface of Ag_2S sheets at room temperature.

Triplicate Ag_2S samples (0.04 g) were dispersed into 40 mL of deionized water separately. Afterwards, 0.5, 1.0, and 1.5 mmol $AgNO_3$ were added, respectively. All solutions were magnetically stirred for 0.5 h. Finally, 1.7, 3.3, and 5.0 mL of Na_3PO_4 solution (0.1mol/L) were added to the corresponding solutions, respectively. The molar ratio of Ag^+ to PO_4^{3-} was 3:1. Three Ag_3PO_4/Ag_2S composites were collected and washed by deionized water and absolute alcohol, then dried in vacuum at 30°C for a whole night. The molar ratios of Ag_2S to Ag_3PO_4 were calculated to be 0.9, 0.47, and 0.31, respectively. Therefore, the corresponding samples were designated as AA0.9, AA0.47, and AA0.31.

For comparison, pure Ag_3PO_4 sample was obtained by directly mixing of 40 mL of $AgNO_3$ solution (1.5 mM) and 5 mL of Na_3PO_4 solution (0.1 M). Ag_3PO_4@Ag_2S sample was prepared by mixing pure Ag_3PO_4 sample with Na_2S solution (0.1 M) for 1min.

2.3 Characterization

The crystal structure of the composite catalysts was analysed by X-ray diffraction (XRD) patterns using a Rigaku D/max-III A diffractometer. The morphologies of the as-synthesized samples were observed using JSM-5610LV scanning electron microscope (SEM). The Fourier Transform Infrared (FTIR) spectra were obtained with a Nicolet 360 spectrometer. UV-Vis absorption spectra were recorded on a UV2550 spectrophotometer.

2.4 Photocatalytic activity test

The photocatalytic activity tests were conducted under visible light irradiated by a 300 W Xe lamp with a UV filter. In every experiment, 0.02 g of photocatalyst (e.g., pure Ag_3PO_4 particles, bare Ag_2S powder, or some Ag_3PO_4/Ag_2S composites) was placed in a Petri dish containing 20 mL of RhB solution (1×10^{-5} mol/L) at room temperature. The solution was magnetically stirred in the dark place for 0.5 h to reach the adsorption-desorption equilibrium between the catalyst and the RhB dye. During photocatalysis, the solution was continuously stirred. 3.0 mL of the solution was suctioned at a regular time interval and centrifuged to remove the precipitates, and the supernatant was analysed using UV-Vis absorption spectra. The photocatalytic degradation behaviour

of RhB dye was obtained by recording the variation of its absorption spectrum as a function of irradiation time.

The detection experiments concerning oxidizing species in the catalytic processes were also conducted by adding the quencher and scavenger of •OH, $O_2^{\bullet-}$ and H^+ into the RhB solution prior to the photocatalyst.

3. Results and discussion

3.1 Characteristics of microstructure of Ag_3PO_4/Ag_2S composites

The Ag_2S template was prepared via cation-exchange reaction between ZnS (en) hybrid and $AgNO_3$ solution. The structure of the as-prepared template was examined. As seen in Fig.2a, the XRD pattern identifies the template as monoclinic α-Ag_2S (JCPDF 14-0072). The related FTIR spectrum indicates that partial amino-groups were kept after ZnS was replaced by Ag_2S, which can attract Ag^+ and induce the nucleation of Ag_3PO_4 on the surface of Ag_2S (Fig. S1). Figs. 2b-d show the XRD patterns of Ag_3PO_4/Ag_2S composites with different molar ratio of Ag_2S to Ag_3PO_4, indicative of the combination of Ag_3PO_4 and Ag_2S. The diffraction peaks marked with diamonds are assigned to monoclinic α-Ag_2S and the other peaks correspond to body-centred cubic phase Ag_3PO_4 (JCPDS No. 06-0505). No peaks corresponding to Ag or other impurities were detected. It is clear that with the increase of the content of Ag_3PO_4, the intensity of the diffraction peaks of Ag_3PO_4 enhances accordingly.

Typical SEM image of blank Ag_2S (Fig.3a) clearly indicates that the synthetic method offers high-yield production of micrometre-sized Ag_2S sheets with a thickness close to 100 nm. The obtained Ag_2S sheets are porous, similar to the morphologies of ZnS(en)-derived CdS and CuS sheets.[29] For the Ag_2S sheets, the remarkable disparity of the solubility product constant between ZnS and Ag_2S makes it possible to completely replace Zn^{2+} with Ag^+. In this process, higher temperature is necessary. Therefore, the abundant voids in Ag_2S sheets originated from the decomposition of ZnS(en) and the large lattice mismatch between ZnS and Ag_2S.[30] Figs. 3b-d exhibit the morphological evolution from Ag_2S sheets to several Ag_3PO_4/ Ag_2S samples. For the AA0.9 sample, homogeneous Ag_3PO_4 particles with an average size of 100 nm are decorated on the surface of Ag_2S sheets. It is distinctly observed that these tiny particles are mutually independent, revealing Ag_2S sheets could inhibit the agglomeration of Ag_3PO_4 particles. Pure Ag_3PO_4 samples served as the reference was conducted by mixing 40 mL of 1.5 mM $AgNO_3$ solution and 5 mL of 0.1 M Na_3PO_4 solution. Seen from Fig.S2, some of the irregular particles have a size larger than 500 nm. The differences in morphology indicate that the functional groups on the surface of Ag_2S play a crucial role in inhibiting the growth of Ag_3PO_4 particles and promoting the intimate contact between Ag_3PO_4 nanoparticles and the two-dimensional Ag_2S sheets. It could also be observed that with the increase of the content of Ag_3PO_4 precursor, more Ag_3PO_4 particles were produced. Accordingly, the microstructure and composition of

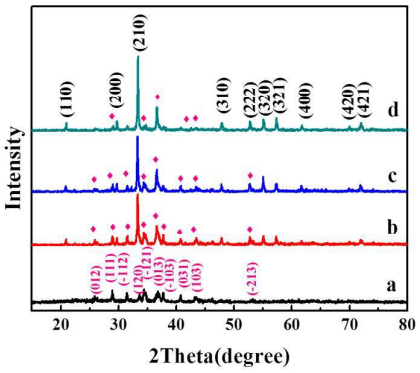

Fig.2 XRD patterns of (a) bare Ag_2S sheets, (b) AA0.9, (c) AA0.47, and (d) AA0.31.

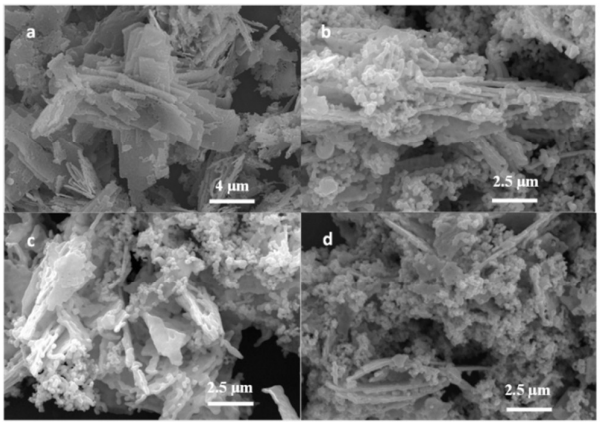

Fig.3 SEM images of (a) bare Ag_2S sheets, (b) AA0.9, (c) AA0.47, and (d) AA0.31.

Ag_3PO_4/Ag_2S composites could be effectively tailored by ZnS(en)-derived Ag_2S sheets.

The interaction of Ag_2S and Ag_3PO_4 in the typical AA0.31 composite was analysed by XPS measurement (Fig.4a). For AA0.31, the signals of Ag, S, P, and O elements were detected, indicating the formation of composite structure. N was not detected due to the removal of partial ethanediamine after the formation of Ag_3PO_4/Ag_2S composite or the covering effect of Ag_3PO_4 nanoparticles. Comparing the high-resolution XPS spectra of Ag3d of pure Ag_3PO_4, bare Ag_2S, and AA0.31, we find that the binding energy of Ag3d of AA0.31 locates between those of pure Ag_3PO_4 and bare Ag_2S (Fig.4b). Relative to pure Ag_3PO_4, the binding energy of P 2P of AA0.31 shifts from 132.601 eV to a higher value of 132.801 eV (Fig.4c). As seen in Fig.4d, the binding energy of S 2P of AA0.31 is higher than that of bare Ag_2S, showing a deviation of about 1.2 eV. The changes of the binding energy of Ag3d, P 2P and S 2P stem from the strong interaction between Ag_2S and Ag_3PO_4 induced by the amino groups on the surface of Ag_2S sheets,

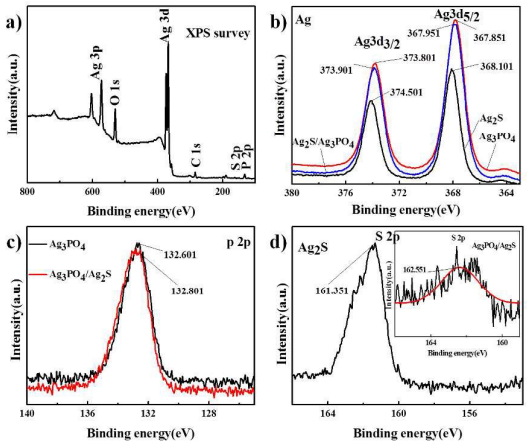

Fig.4 a) XPS survey spectrum of typical Ag_3PO_4/Ag_2S composite (AA0.31). The high-resolution XPS spectra of b) Ag3d of pure Ag_3PO_4, bare Ag_2S and AA0.31, c) P2p of AA0.31 and pure Ag_3PO_4, and d) S2P of bare Ag_2S and AA0.31.

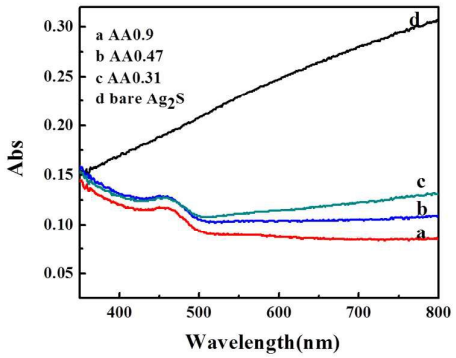

Fig.5. UV–Vis diffuses reflectance spectra of bare Ag_2S sheets, AA0.9, AA0.47, and AA0.31.

which favours the stability of Ag_3PO_4 in aqueous solution.

3.2 Optical properties of Ag_3PO_4/Ag_2S composites

UV–Vis diffuse reflectance spectra of pure Ag_3PO_4, bare Ag_2S sheets and Ag_3PO_4/Ag_2S composites were recorded to analyse the influence of Ag_2S on the absorption of Ag_3PO_4. It can be observed that pure Ag_3PO_4 exhibits a wide adsorption peak in the range of 400-530 nm (Fig. S3). The Ag_2S sheets with a narrow band gap display a significant growth trend with the increase of the wavelength in the range of 530-800nm (Fig.5d). Three Ag_3PO_4/Ag_2S composites exhibit a favourable combination of the two silver compounds in light absorption characteristics. As Ag_2S content increases, the adsorption degree enhances (AA0.9>AA0.47>AA0.31). Therefore, the introduction of narrow- gap Ag_2S sheets improves the light harvesting efficiency of Ag_3PO_4 in the visible-light range.

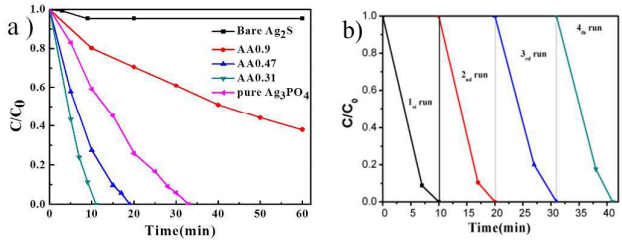

Fig.6 a) Photocatalytic degradation curves of RhB solution over pure Ag_3PO_4, bare Ag_2S and different Ag_3PO_4/Ag_2S composites. b) Recyclability of AA0.31 in four successive photocatalytic experiments.

3.3 The photocatalytic activities of Ag_3PO_4/Ag_2S composites

The photocatalytic activities of pure Ag_3PO_4, bare Ag_2S sheets, and different Ag_3PO_4/Ag_2S composites were compared by degrading RhB dyes under the visible-light irradiation, as shown in Fig.6a. Bare Ag_2S sheets showed weak activity by degrading 5% dyes in 60 min. For pure Ag_3PO_4, the mauve dyes were completely degraded in 33 min. AA0.9 containing higher content of Ag_2S exhibited a performance inferior to pure Ag_3PO_4 by decomposing 40% dyes in 60 min. The photocatalytic efficiency of the composite was enhanced as the proportion of Ag_3PO_4 was increased. Both AA0.47 and AA0.31 showed improved efficiency compared to pure Ag_3PO_4. Specifically, AA0.31 showed about 2-fold enhancement in degradation rate in comparison to pure Ag_3PO_4, accomplishing the degradation process in 11 min. Although the colour of Ag_2S sheets is black, the performances of the three samples were not affected by the light-block effect, which is an unavoidable issue for the utilization of some transition metal sulphides, such as CuS, Ag_2S, FeS, etc., as visible-light-driven photocatalysts.[31] A comparison experiment was conducted by mixing pure Ag_3PO_4 particles with 0.1 M of Na_2S solution for 1 min at room temperature (Ag_3PO_4@Ag_2S, the FESEM image is shown in Fig.S4). After the surface of Ag_3PO_4 was covered by Ag_2S nanoparticles, the photocatalytic activity of Ag_3PO_4 was deteriorated due to the limited visible-light adsorption of black Ag_2S (Fig.S5). Therefore, decorating visible-light photocatalysts on the surface of two-dimensional IR-light-responsive semiconductors can possibly expand the utilization of these semiconductors. However, higher content of Ag_2S in the composite may produce an unsuitable ratio between Ag_2S and Ag_3PO_4, thereby lowering the photocatalytic efficiency (AA0.9). Furthermore, a mechanically mixed sample containing Ag_2S and Ag_3PO_4 was prepared with the same molar ratio of Ag_2S to Ag_3PO_4 as AA0.31. The sample indicated lower activity than pure Ag_3PO_4 and AA0.31, decomposing the dyes in 60 min (Fig.S6). Consequently, the efficient charge transfer at the heterojunction interface is crucial for the improvement of the catalytic performance. It also demonstrates that the synergistic effect between Ag_2S and Ag_3PO_4 plays important roles in improving the photocatalytic activity.

We also prepared Ag_3PO_4/Ag_2S composite in the absence of en according to the preparation method in the previous paper[31]. Without en, the Ag_3PO_4/Ag_2S sample could degrade the dye in 19min (Fig.S7). Therefore, the degradation time was longer than that of Ag_3PO_4/Ag_2S composite in the presence of NH_2. It indicates that NH_2 groups can promote electron transfer [32]and improve the performance of the Ag_3PO_4-based photocatayst.

Rh B sensitization has important influence on the dye degradation. Therefore, we also used phenol as the colourless compound to detect the performance of Ag_3PO_4/Ag_2S photocatalysts. AA0.31 decomposed 60% phenol in 300min (Fig.S8). The result indicates that the high-efficiency performance of Ag_3PO_4/Ag_2S is not only related with the Rh B sensitization but with the photocatalysis performance of the Ag_3PO_4/Ag_2S composite.

The used AA0.31 was collected and dispersed into the fresh dye solution to measure the stability of the composite in the photocatalysis process .The process was repeated three times. In the second and third run, though the colour of the catalyst became darker, the used catalyst held the original activity, suggesting that AA0.31 could be used for four times and keep activity for at least 45 min under the visible-light irradiation (Fig.6b). Obviously, the stability of Ag_3PO_4/Ag_2S composite surpasses that of pure Ag_3PO_4(Fig.S9)[33].

3.4 Mechanism of photodegradation over Ag_3PO_4/Ag_2S composites

Active species trapping experiments were performed to discern the essential reasons for the superior performance of Ag_3PO_4/Ag_2S composites. Tert-butanol, benzoquinone (BZQ) and EDTA-2Na served as the scavengers of •OH, $O_2^{\bullet-}$ and h^+, respectively. Fig.7a shows the photocatalytic curves of RhB solution over AA0.31 with different scavengers. It is apparent that tert-butanol did not change the degradation rate of RhB. Therefore, •OH active species did not occur on the surface of AA0.31 under the visible light. Degradation efficiencies of 68% and 30% were reduced after BZQ and EDTA-2Na were added, respectively. Therefore, it is concluded that $O_2^{\bullet-}$ and h^+ were effective in decomposing dyes. For pure Ag_3PO_4, h^+ was the only active substance. The Ag^+ on the surface of Ag_3PO_4 can capture the photogenerated electrons, leading to the formation of Ag. The conduction band (CB) potential of Ag_3PO_4 is lower than that of $O_2/ O_2^{\bullet-}$ redox couple (+0.13 eV vs. NHE) [34].Therefore, the photogenerated electrons could not be accepted by O_2. However, in the catalytic process over AA0.31, $O_2^{\bullet-}$ species appeared and were effective in decomposing dyes, which meant the photogenerated electrons from Ag_2S sheets participated in the one-electron reduction reaction.

The band structure of Ag_3PO_4/Ag_2S was analysed to investigate its catalytic mechanism thoroughly. The CB and valence band (VB) of Ag_2S were estimated according to the following equations:

$$E_C = -(\chi(A)^a \cdot \chi(B)^b \cdot \chi(C)^c)^{1/(a+b+c)} + \frac{1}{2}E_g + E_0$$

$$E_V = E_C + E_g$$

where E_V is the valence band edge potential; χ is the electronegativity of the semiconductor, which is the geometric mean of the electronegativity of the constituent atoms; and E_0 is the energy of free electrons on the hydrogen scale (about 4.5 eV vs. NHE). E_g of Ag_2S is 1.0 eV. Therefore, the E_C and E_V of Ag_2S are 0.04 and 1.04 eV, respectively.

The band structure of Ag_3PO_4/Ag_2S composite is plotted in Fig.8. Under visible-light irradiation, both Ag_3PO_4 and Ag_2S can be excited, and the photogenerated electrons and holes are distributed in their conduction and valence bands, respectively. The VB of Ag_3PO_4 has a positive value of 2.9 eV, which means that the photogenerated holes have strong oxidation ability. In thermodynamics, the holes can transfer from Ag_3PO_4 to Ag_2S, thereby facilitating the separation of photogenerated electrons and holes. However, the oxidation ability of h^+ stayed at the VB of Ag_2S (1.04 eV vs. NHE) is too weak to decompose dyes. Consequently, the holes utilized to decompose the dyes are mainly donated by Ag_3PO_4. Furthermore, the electrons located on the CB of Ag_2S (0.04 eV vs. NHE) react with O_2 to form $O_2^{\bullet-}$, which can also oxidize the dyes. In this case, partial photocatalysis reactions proceed on the surface of the porous Ag_2S sheets that possess a great amount of active sites. According to the report in literature, [33] the work function of excited RhB is -3.08 eV. It means that the photogenerated electrons from excited dyes can transfer to Ag_2S, and then take part in the photocatalysis process. Therefore, more $O_2^{\bullet-}$ could be produced.

Additionally, the interfacial effect produced by monodispersed Ag_3PO_4 nanoparticles and Ag_2S sheets can transfer the photogenerated electrons or holes to the surface quickly and accelerate the oxidation reactions.

For the double silver compounds system, under the visible-light irradiation, a small quantity of Ag was unavoidably produced. The direct proof is the XRD pattern of the used AA031 sample after the first photocatalytic test (Fig.S10). In order to elucidate the photocatalytic mechanism of the Ag_3PO_4/Ag_2S photocatalyst, AA0.31 before and after 1 cycle have been characterized by EDS, and the results are listed in Table 1. We can find that the atom content of Ag is increased for the used AA 0.31, compared to that of original sample and it is higher than the sum of the duple of S and triple P, implying the formation of metallic Ag.

The plasma effects of metallic Ag particles can also improve the photocatalysis efficiency of Ag_3PO_4 [35]. The Fermi energy of Ag proved more positive than the CB level of Ag_3PO_4 and more negative than VB of Ag_2S. Therefore, Ag formed at the interface of Ag_3PO_4/Ag_2S after the initiation of the photocatalysis process and acted as the combination sites for the fast combination between the photoexcited holes at the VB of Ag_2S and photoexcited electrons in the CB of Ag_3PO_4. [36] Therefore, in this composite system, the catalytic behaviour complies with the Z-scheme photocatalytic mechanism. The electrons at the CB of Ag_2S react with molecular oxygen to form $O_2^{\bullet-}$ species that have the ability of oxidizing RhB, while the holes at the VB of Ag_3PO_4 oxidize RhB directly.

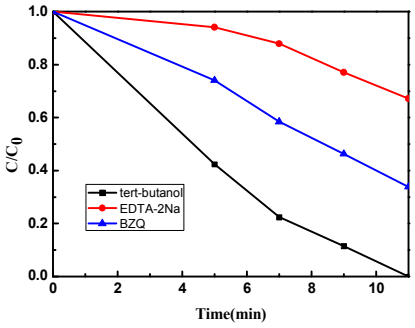

Fig.7 Photocatalytic degradation curves of RhB solution over AA0.31 with the addition of tert-butanol, EDTA, and benzoquinone, respectively.

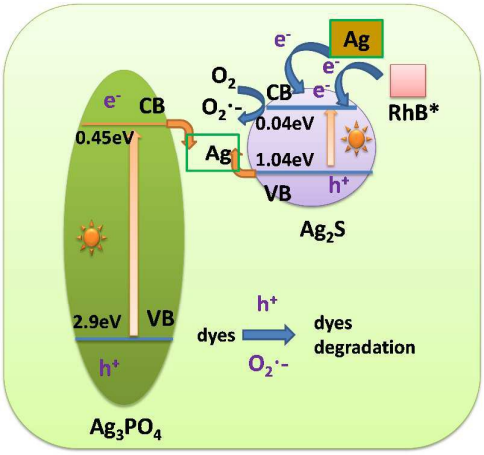

Fig.8. Photocatalytic mechanism scheme of Ag_3PO_4/Ag_2S composites under visible-light irradiation.

4. Conclusions

High-performance photocatalysts were obtained by depositing Ag_3PO_4 nanoparticles on the surface of two-dimensional Ag_2S sheets via in- situ synthesis strategy at room temperature. The microstructure, composition, and performance of the resulting Ag_3PO_4/Ag_2S composites can be tailored by adding different ratio of Ag_2S sheets. Ag_3PO_4/Ag_2S composite reached optimum performance when the molar ratio of Ag_2S to $Ag_3PO_4$was 0.31. In the Ag_3PO_4/Ag_2S composite system, $O_2^{\bullet-}$ species derive from the electrons in the CB of Ag_2S and holes in the VB of Ag_3PO_4 have strong oxidation ability. Therefore, the photocatalysis process corresponds with the Z-scheme photocatalytic mechanism. Due to the advantageous interface produced by two-dimensional Ag_2S sheets and nano Ag_3PO_4 particles, efficient light harvesting and matched band structure of Ag_2S and Ag_3PO_4 contribute to the superior photocatalytic activity.

Acknowledgements

This work was financially supported by the National Natural Science Foundation of China (51161140399), the Ministry of Science and Technology of China (2015DFR50650), and the Fundamental Research Funds for the Central Universities (WUT: 2015IB002).

Notes and references

1 Z. Yi, J. Ye, N. Kikugawa, T. Kako, S. Ouyang, H. Stuart-Williams, H. Yang, J. Cao, W. Luo, Z. Li, Y. Liu and R. L. Withers, Nature materials, 2010, 9, 559-564.
2 D. J. Martin, G. Liu, S. J. Moniz, Y. Bi, A. M. Beale, J. Ye and J. Tang, Chem Soc Rev, 2015, DOI: 10.1039/c5cs00380f.
3 H. C. Zhang, H. Huang, H. Ming, H. T. Li, L. L. Zhang, Y. Liu and Z. H. Kang, J Mater Chem, 2012, 22, 10501-10506.
4 X. F. Yang, H. Y. Cui, Y. Li, J. L. Qin, R. X. Zhang and H. Tang, Acs Catal, 2013, 3, 363-369.
5 Z. Jiao, Y. Zhang, H. Yu, G. Lu, J. Ye and Y. Bi, Chem Commun (Camb), 2013, 49, 636-638.
6 Y. He, L. Zhang, B. Teng and M. Fan, Environmental science & technology, 2015, 49, 649-656.
7 S. Kumar, T. Surendar, A. Baruah and V. Shanker, Journal of Materials Chemistry A, 2013, 1, 5333-5340.
8 L. L. Zhang, H. C. Zhang, H. Huang, Y. Liu and Z. H. Kang, New J Chem, 2012, 36, 1541-1544.
9 J. J. Guo, S. X. Ouyang, H. Zhou, T. Kako and J. H. Ye, J Phys Chem C, 2013, 117, 17716-17724.
10 X.J. Guan and L.J. Guo，Acs Catal, 2014, 4, 3020−3026.
11 G. Q. Luo, X. J. Jiang, M. J. Li, Q. Shen, L. M. Zhang and H. G. Yu, Acs Appl Mater Inter, 2013, 5, 2161-2168.
12 M. S. Zhu, P. L. Chen and M. H. Liu, Langmuir, 2012, 28, 3385-3390.
13 Q. Li, B. D. Guo, J. G. Yu, J. R. Ran, B. H. Zhang, H. J. Yan and J. R. Gong, J Am Chem Soc, 2011, 133, 10878-10884.
14 F. K. Meng, J. T. Li, S. K. Cushing, J. Bright, M. J. Zhi, J. D. Rowley, Z. L. Hong, A. Manivannan, A. D. Bristow and N. Q. Wu, Acs Catal, 2013, 3, 746-751.
15 R. F. Zhou and S. Z. Qiao, Chem Mater, 2014, 26, 5868-5873.
16 S. W. Baek, G. Park, J. Noh, C. Cho, C. H. Lee, M. K. Seo, H. Song and J. Y. Lee, Acs Nano, 2014, 8, 3302-3312.
17 H. T. Ren, S. Y. Jia, Y. Wu, S. H. Wu, T. H. Zhang and X. Han, Ind Eng Chem Res, 2014, 53, 17645-17653.
18 J. Zhuang, W. Lai, M. Xu, Q. Zhou and D. Tang, ACS Appl Mater Interfaces, 2015, DOI: 10.1021/acsami.5b01923.
19 D. Jiang, L. Chen, J. Xie and M. Chen, Dalton Trans, 2014, 43, 4878-4885.
20 L. Huang, H. Xu, Y. Li, H. Li, X. Cheng, J. Xia, Y. Xu and G. Cai, Dalton Trans, 2013, 42, 8606-8616.
21 S. Khanchandani, P. K. Srivastava, S. Kumar, S. Ghosh and A. K. Ganguli, Inorg Chem, 2014, 53, 8902-8912.
22 Z. C. Shan, D. Clayton, S. L. Pan, P. S. Archana and A. Gupta, Journal of Physical Chemistry B, 2014, 118, 14037-14046.
23 C. H. Fang, Y. H. Lee, L. Shao, R. B. Jiang, J. F. Wang and Q. H. Xu, Acs Nano, 2013, 7, 9354-9365.
24 H. L. Wang and L. M. Qi, Adv Funct Mater, 2008, 18, 1249-1256.
25 P. Leidinger, R. Popescu, D. Gerthsen and C. Feldmann, Chem Mater, 2013, 25, 4173-4180.
26 Y. Lei, H. M. Jia, W. W. He, Y. G. Zhang, L. W. Mi, H. W. Hou, G. S. Zhu and Z. Zheng, J Am Chem Soc, 2012, 134, 17392-17395.
27 L. Yang, H. Y. Yang, Z. X. Yang, Y. X. Cao, X. M. Ma, Z. S. Lu and Z. Zheng, Journal of Physical Chemistry B, 2008, 112, 9795-9801.
28 L. Nasi, D. Calestani, T. Besagni, P. Ferro, F. Fabbri, F. Licci and R. Mosca, J Phys Chem C, 2012, 116, 6960-6965.
29 J. Zhang, J. Yu, Y. Zhang, Q. Li and J. R. Gong, Nano Lett, 2011, 11, 4774-4779.

30 Y. F. Yu, J. Zhang, X. Wu, W. W. Zhao and B. Zhang, Angew Chem Int Edit, 2012, 51, 897-900.
31 J.T.Tang, W.Gong, T.J. Cai, T. Xie, C. Deng, Z.S. Peng and Q. Deng, RSC Adv., 2013, 3, 2543–2547.
32 H.Katsumata, H. Ando, T.Suzuki and S.Kaneco, Ind. Eng. Chem. Res. 2015, 54, 3532−3535.
33 P. Ma, A. Chen, Y. Wu, Z. Fu, W. Kong, L. Che and R. Ma, J Colloid Interface Sci, 2014, 417, 293-300.
34 M.Ge, N.Zhu Y.P. Zhao, J.Li, and L.Liu, Ind. Eng. Chem. Res. 2012, 51, 5167−5173.
35 Y.P. Liu, L. Fang, H.D.Lu, L.J.Liu , H. Wang, and C.Z. Hu, Catalysis Communications 2012, 17,200–204.
36 H. Katsumata, T. Sakai, T. Suzuki and S. Kaneco, Ind Eng Chem Res, 2014, 53, 8018-8025.